Applied Catalysis A: General 518 (2016) 206–212

Contents lists available at ScienceDirect

Applied Catalysis A: General

journal homepage: www.elsevier.com/locate/apcata

Photocatalytic methanol assisted production of hydrogen with simultaneous degradation of methyl orange

Joana Romão, Rafal Salata, Sun-Young Park, Guido Mul*

Photocatalytic Synthesis Group, MESA+ Institute for Nanotechnology, Faculty of Science and Technology, University of Twente, Meander 229, P.O. Box 217, 7500 AE Enschede, The Netherlands

ARTICLE INFO

Article history:
Received 26 June 2015
Received in revised form 12 October 2015
Accepted 14 October 2015
Available online 17 October 2015

Keywords:
Photocatalysis
Hydrogen
Platinum
Titanium dioxide
Methyl orange
Methanol
Decontamination
Oxidation
Anaerobic conditions

ABSTRACT

Platinized TiO_2 prepared by photodeposition was evaluated for activity in the simultaneous conversion of methyl orange (MO), and methanol assisted formation of hydrogen. Low concentrations of MO were found ineffective for generation of hydrogen in measurable quantities upon illumination of Pt/TiO_2 in water. On the other hand, methanol induced hydrogen formation was significant. Surprisingly, when methyl orange was added to the methanol/water solution, hydrogen formation was significantly suppressed. The origin of this detrimental effect of methyl orange lies in the strong and preferred adsorption of the dye on the Pt sites of the catalyst, resulting in hydrogenation of the azo bond and suppression of the catalyzed formation of hydrogen. The hydrogenation of the azo bond is corroborated by dis-colorization of the solution and the observation of a mass fragment in LC–MS analysis corresponding to a hydrogenated product of MO (m/z = 172). Similar to hydrogen formation, dye dis-colorization is stimulated by the presence of methanol, without the formation of new chemical compounds, confirming the role of methanol as a hole scavenger in the photocatalytic processes. Finally the presence of oxygen (in lean conditions) delays dye hydrogenation and hydrogen formation, which we discuss is due to oxygen adsorption and formation of superoxide anions over the Pt sites (leading to oxidation of methanol), which is preferred over N=N bond hydrogenation, and proton reduction.

1. Introduction

Potable water in several domestic areas not only contains organic toxins, but also significant amounts of nitrate, which both have adverse effects on human health [1,2]. To mitigate these issues, photocatalysis is a promising technology, in particular if oxidation of organic toxins to CO_2 [3,4], could be combined with the in situ generation of hydrogen [5,6], needed for reductive elimination of nitrate by heterogeneous catalysis [7]. Both reactions (generation of hydrogen, and reductive elimination of nitrates) could e.g. be performed sequentially in domestic appliances, designed on the basis of microreactor technology [7].

The photocatalytic process of oxidative decomposition of organics and hydrogen formation by reduction of protons, involves photo-excited states, i.e. electrons and holes (see for a schematic illustration Fig. 1) [8,9]. Photogenerated holes when reaching the semiconductor surface induce the formation of radical species, such as hydroxyl radicals, or organic radicals by reaction with surface adsorbed organic compounds (Fig. 1). Usually conversion of the radical species and organic contaminants subsequently leads to formation of CO_2 and H_2O [4,8]. Several reports demonstrate that such decomposition of contaminants is feasible in anaerobic conditions, with simultaneous formation of hydrogen (Fig. 1) [10,11].

The catalyst most commonly used to induce the above illustrated reactions, is TiO_2 (and specifically P25) [12,13], with a bandgap of 3.2 eV and a conduction band (E_{CB}) energy lower than the standard redox potential of hydrogen (E (H^+/H_2) 0 V at pH 0), which makes hydrogen production thermodynamically feasible [14]. Unfortunately, hydrogen evolution is usually associated with low apparent quantum efficiency [8]. The reason is a high recombination rate between the photogenerated holes and electrons, before achieving the desired redox processes on the semiconductor surface [8]. This problem can be overcome by loading TiO_2 with noble metals, such as Pt, Pd, Au, Cu, or Rh [8,9,14,15]. These metals create effective surface sites for proton reduction, thus diminishing recombination of electrons and holes [14].

Decomposition of several organic compounds has been studied in anaerobic conditions, leading to production of hydrogen [16,17], such as alcohols [16,18], sugars [19], organic acids [16,20], and others [5,21]. Alcohols are the organic compounds that induced the

* Corresponding author. Fax: +31 53 489 2882.
E-mail address: g.mul@utwente.nl (G. Mul).

http://dx.doi.org/10.1016/j.apcata.2015.10.020
0926-860X/

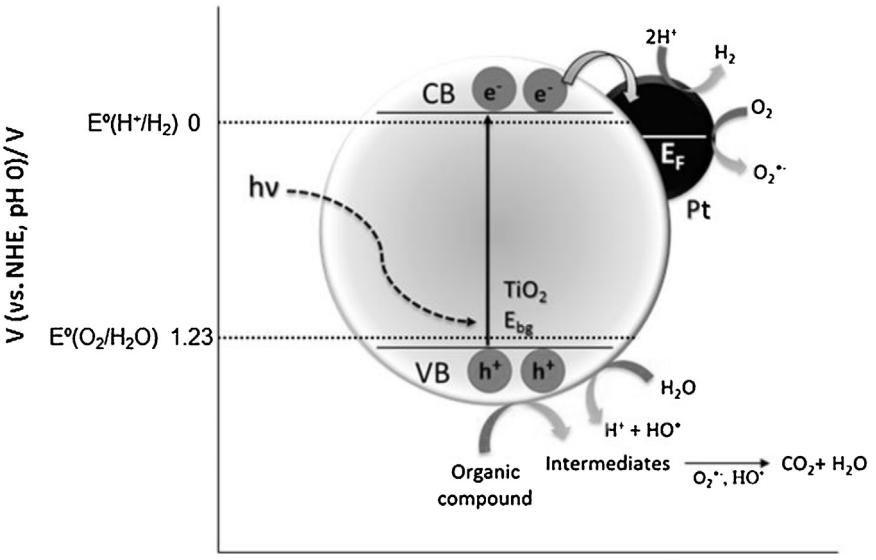

Fig. 1. Schematic illustration of TiO_2 loaded with Pt, and the processes occurring which are relevant for photocatalytic decomposition of organic compounds with simultaneous H_2 production.

highest rates in hydrogen evolution, likely due to their high susceptibility towards adsorption on oxidic surfaces and subsequent oxidation [22].

The aim of this paper is to demonstrate the effectivity of Platinized TiO_2 (P25) in the decomposition of methyl orange (MO), a dye that is often used as model compound in studies involving decontamination of wastewater, and the simultaneous production of hydrogen in the presence of excess MeOH. MeOH is known to induce hydrogen evolution very efficiently [9]. Both anaerobic, and oxygen lean conditions will be discussed, the latter condition representing water to be purified in domestic appliances.

2. Experimental

2.1. Materials

All reagents were obtained from Aldrich and used as received. Those include chloroplatinic acid, methanol and methyl orange. The photocatalyst material, P25 TiO_2, was obtained from Evonik Industries. The solvents (water and acetonitrile) used in the HPLC analysis were purchased from Biosolve.

2.2. Preparation of Pt-TiO_2

Deposition of Pt nanoparticles on TiO_2 P25 with an estimated weight loading of 0.5 wt-% was performed using a photodeposition procedure [23,24]. To this end, an aqueous suspension of TiO_2 P25 (0.5 g l^{-1}) and chloroplatinic acid (H_2PtCl_6, 0.5 g l^{-1}) was stirred for 30 min in the dark and then MeOH was added (1 M, 3 ml). The suspension was illuminated (radiation intensity 3.21 mW cm^{-2} at 375 nm) for 5 h. The powder was collected by centrifugation, and washed three times consecutively with ethanol (20 ml), and finally with distilled water (20 ml). The powder was dried overnight at 90 °C.

2.3. Photocatalytic experiments

The equipment used for photocatalytic reactivity evaluation consists of three parts: a reactor, a gas chromatograph and a Lab-

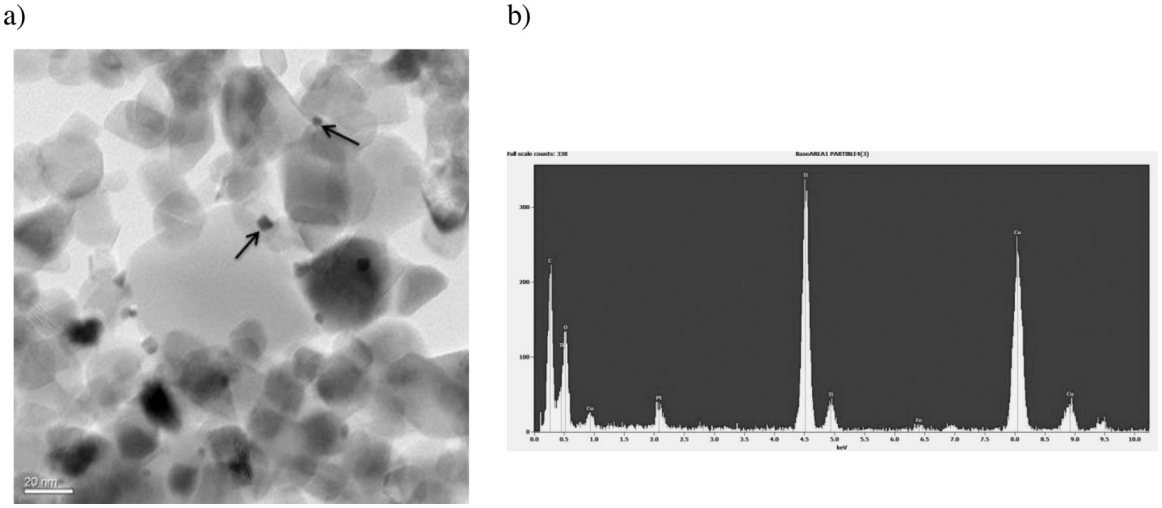

Fig. 2. Characterization of 0.5 wt-% Pt-P25. (a) TEM image with several Pt particles indicated by the arrows, and (b) an exemplary EDX spectrum of the particles, identifying the presence of Pt.

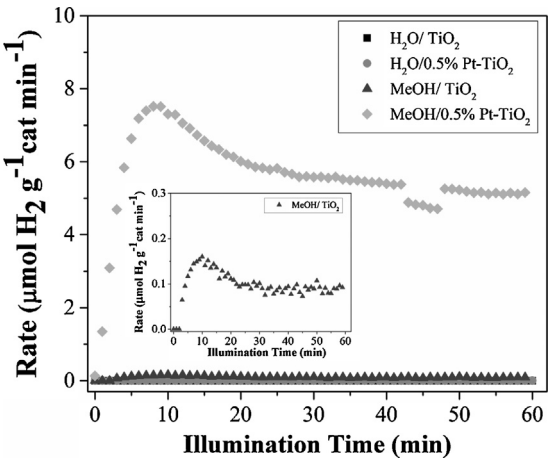

Fig. 3. Hydrogen concentration as determined in a CSTR for TiO_2 and 0.5% Pt/TiO_2 photocatalysts from aqueous suspensions with (2.58 M) or without MeOH, as a function of illumination time. The inset shows a magnification of the result obtained for MeOH with TiO_2.

View interphase to control gas flow rates induced by mass flow controllers. A cylindrical batch reactor was used with an internal volume of 50 ml. In the lid of the reactor a small window (fused silica of 0.5 cm diameter, which allows 90% transmission of radiation) was incorporated, to allow illumination of the solution from the top. The light source used was a 120 W high pressure mercury lamp from Dr. Gröbel UC-Elektronik GmbH, with a spectral range from 280 to 650 nm, from which the light was introduced in the reactor through an optical fiber at a light intensity of 82 mW cm^{-2} (measured from 300 to 400 nm, at a distance from the window of 1 cm). A micro gas chromatograph (GC), equipped with a Parabond Q column (10 m) and a TCD detector was used for the determination of H_2, O_2 and N_2 concentrations [25]. The working volume of the aqueous photocatalytic suspension was 15 ml, which was continuously agitated by magnetic stirring at 300 rpm. In this study several aqueous solutions were prepared to compare photocatalytic activity, including MeOH (2.48 M, or otherwise as stated) or mixtures of MeOH (2.48 M) and methyl orange (MO), (0.06 mM, or otherwise as stated). All reactions were performed at neutral pH (~7). Two photocatalysts were tested with a concentration of 1 g l^{-1}, being TiO_2 and 0.5% Pt–TiO_2. Before initiating the photocatalytic reaction, the aqueous solution was purged with argon, or argon containing 20% O_2 (5 ml min^{-1}, to saturate the aqueous solution with O_2), for 30 min in the dark. The total time of illumination was 60 min during which an argon (Ar) flow of 5 ml min^{-1} was continuously purged through the reactor.

2.4. Analysis of MO decomposition

From the same reactor used for determination of hydrogen production, samples were taken out periodically and centrifuged at 7000 rpm for 5 min to remove catalyst particles. Subsequently the samples were analyzed by UV–vis spectroscopy and liquid HPLC (Agilent 1100 Series). The HPLC method involved the separation of the organic compounds in the sample using a mixture of water and acetonitrile (75:25) as eluent, and applying a flow rate of 0.3 ml min^{-1}. The sample volume injected into the reverse phase column (All Chromolith Merk C18 column 100 mm × 3 mm i.d.) was 10 μL at room temperature (21 °C), using an autosampler. Detection was performed using mass spectrometry (Bruker MS Esquire 3000+). The separated products were ionized using positive Electrospray Ionization (+ESI). The MS ionization conditions were: a flow rate of 0.5 ml min^{-1}, a nebulizer gas pressure of 30 psi, a dry gas flow of 0.3 l min^{-1}, and a dry gas temperature of 325 °C.

3. Results

3.1. Characterization of 0.5% Pt–TiO_2

The Pt–TiO_2 sample was analyzed by X-Ray Fluorescence (XRF, Bruker S4 Pioneer) in order to quantify the platinum loading. The loading determined by XRF amounted to 0.44 wt%. The particle size of Pt was determined by transmission electron microscopy (TEM, Philips CM300ST-FEG) and the composition of the presumably Pt particles confirmed by Energy Dispersive X-ray spectroscopy (EDX, Noran System Six). The results of the TEM and EDX analyses are shown in Fig. 2. From the TEM micrograph a Pt particle size variable between 3 and 5 nm could be determined (Fig. 2a).

3.2. Effect of Pt deposition on hydrogen production activity of TiO_2

Fig. 3 shows the results obtained from the illumination of aqueous suspensions with and without methanol in the presence of two photocatalysts (TiO_2 and 0.5% Pt/TiO_2). In the absence of methanol, hydrogen production was not observed for both

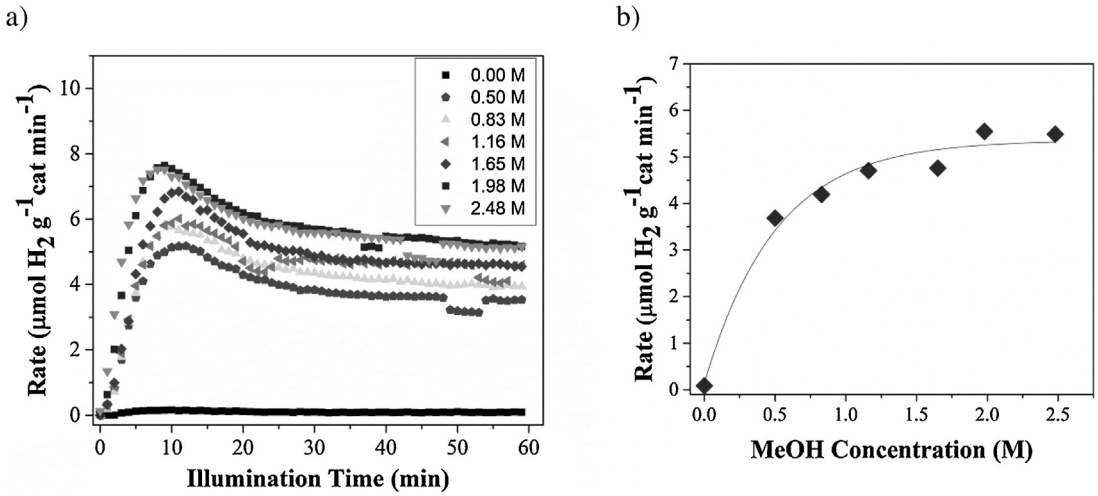

Fig. 4. (a) Time dependent hydrogen concentration determined for 0.5% Pt/TiO_2 catalyst as a function of initial MeOH concentration. (b) Rate constant values found for hydrogen evolution at increasing initial MeOH concentrations (M) showing an exponential trend.

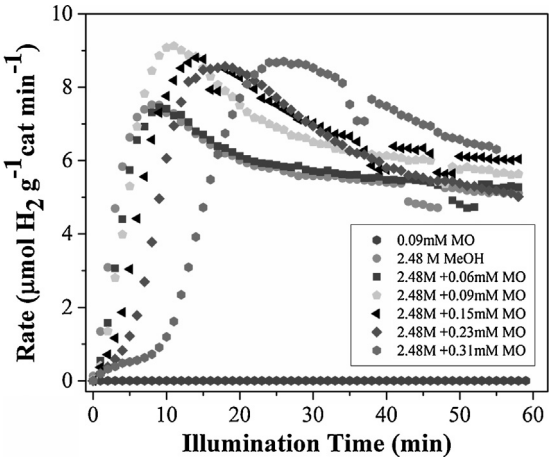

Fig. 5. MeOH (2.48 M) induced hydrogen concentration transients over 0.5% Pt/TiO_2 as a function of the initial MO concentration (varied between 0.06 and 0.31 mM).

catalyst compositions. From the aqueous solution with MeOH (2.48 M) hydrogen evolved in measureable quantities significantly higher for the Pt/TiO_2 catalyst than for the TiO_2 catalyst (see insert for the trend in activity). The initial rise in concentration is due to non-steady state behavior (flush out) of the continuously stirred tank reactor, (CSTR), which requires approximately 10 min. Then a steady state in hydrogen rate of approximately 0.1 μmol $H_2\,g^{-1}{}_{cat}\,min^{-1}$ is reached for TiO_2, although initially the rate is somewhat higher. The initial rate induced by 0.5% Pt/TiO_2 amounts to 7.5 μmol $H_2\,g^{-1}{}_{cat}\,min^{-1}$, which slowly decays to a steady state rate of 5.5 μmol $H_2\,min^{-1}\,g^{-1}{}_{cat}$ (Fig. 3). The Apparent Quantum Efficiency (AQE), taking into account a flux of photons of about 3.25×10^{-5} mol min^{-1}(calculated on the basis of 82 mW cm^{-2} light intensity, 0.5 cm window diameter, and an average wavelength of 365 nm (the dominant mercury emission line in the UV), and an average rate of hydrogen production of 8.25×10^{-8} mol min^{-1}(based on 15 mg of catalyst), amounts to approximately 5.5% (assuming 2 photons are required per mole of H_2).

3.3. Effect of process parameters on H_2 production in anaerobic conditions

3.3.1. Effect of the initial MeOH concentration

Different initial concentrations of MeOH were used in order to determine the optimum for hydrogen production (Fig. 4). For all MeOH concentrations tested, an initial maximum in hydrogen production rate can be observed (after about 10 min), followed by a significant decrease in rate until steady state is reached, variable in quantity for each initial MeOH concentration. Fig. 4b shows that the hydrogen formation rate initially strongly depends on the MeOH concentration, which dependency exponentially decays to close to zero order at MeOH concentrations above approximately 1 M. These phenomena are similar to those reported by Patsoura et al. [17]. In view of the constant rates observed in the CSTR, we do not expect significant deactivation of the catalyst. Fig. 4 also indicates the experiments are fairly reproducible at high methanol concentrations, since for every different methanol concentration a fresh amount of catalyst was used.

3.3.2. Effect of MO on MeOH induced hydrogen formation

The effect of MO on the MeOH induced hydrogen production rate was determined for various MO concentrations, at a fixed concentration of MeOH of 2.48 M. The results of these experiments are summarized in Fig. 5. First, in the absence of MeOH, hydrogen production was below the detection limit of the TCD detector. Apparently MO is not able to stimulate hydrogen formation over Pt/TiO_2 to a significant degree at the concentration levels tested (0.09 M). Further, at a low concentration of 0.06 M, the presence of MO had very little effect on the MeOH induced hydrogen production. However, increasing MO concentration, some remarkable changes were observed. First, the hydrogen formation appears to be delayed and the delay time increases as a function of MO concentration. The maximum hydrogen concentration peak is observed at minute 8 for 0.06 and 0.09 mM, and shifts to minute 23 at the highest concentration of methyl orange (0.31 mM). Second, the maximum in amount of hydrogen produced is higher in the presence of MO, while the transient reaching steady state levels also requires somewhat longer times. The peak in hydrogen production rate obtained in the presence of MO equals to about 9 μmol $H_2\,g^{-1}{}_{cat}\,min^{-1}$.

In order to determine the photocatalytic decomposition of MO, samples were collected after certain illumination intervals and analyzed by UV–vis spectroscopy and LC–MS. The results of MO mineralization in the absence or presence of MeOH are shown in Fig. 6a. After 10 min of illumination full dis-colorization of MO was achieved, while in the presence of MeOH this required even less time. To identify potential compounds formed from MO in the applied anaerobic conditions, LC–MS analysis was performed. A species with m/z of 172 (Fig. 6b) was obtained after 10 min of illumi-

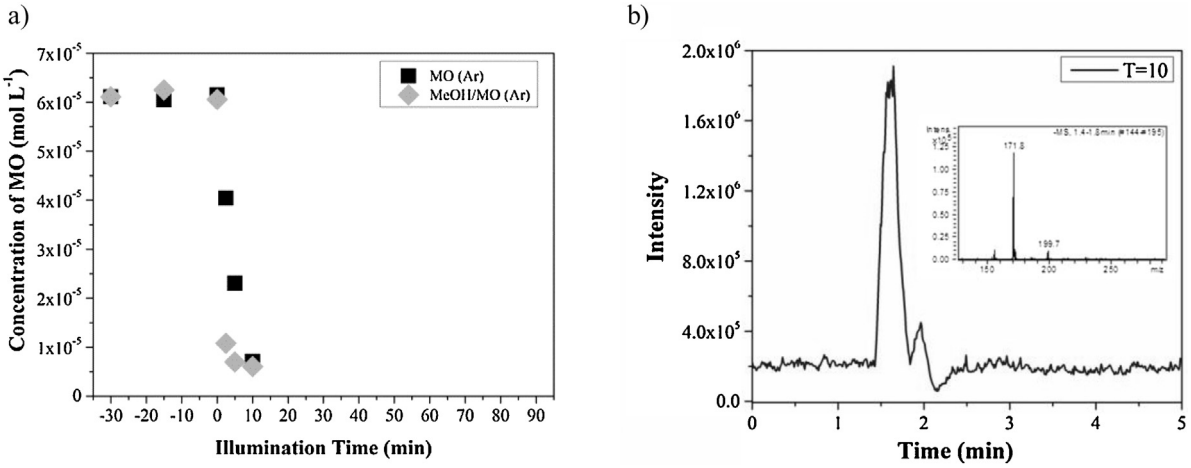

Fig. 6. (a) Photocatalytic dis-colorization of MO (0.09 mM) in the absence or presence of MeOH (2.48 M) in anaerobic conditions (Ar). (b) Analysis by LC–MS of samples at t = 10 min, showing the formation of a compound with a mass fragment of 172 m/z.

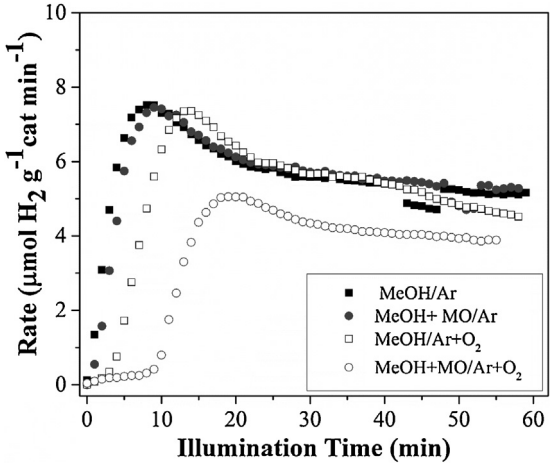

Fig. 7. Hydrogen production over 0.5% Pt/TiO_2 from aqueous suspensions with MeOH (2.48 M) and MO (0.06 mM), as a function of illumination time, comparing anaerobic (Ar) and aerobic (Ar + O_2) conditions.

nation, which we could assign to the formation of a hydrogenated fragment of MO, to be discussed later.

3.4. Quantification of H_2 production in oxygen lean conditions

As stated in the introduction, photocatalytic hydrogen production is likely very much dependent on the presence or absence of oxygen in the water feed. In purification devices to be applied in practice, the water feed will likely contain oxygen (air). It is therefore relevant to study the effect of solved oxygen on the transients described in Fig. 5. To introduce oxygen in the solution, argon with 20% volume of O_2 was purged for 30 min prior to starting illumination. During illumination the purge consisted again of pure Ar. Fig. 7 shows the effect of dissolved oxygen on the MeOH induced hydrogen production transients, in the absence or presence of MO. Clearly, in the absence of MO, the presence of oxygen (□) induces a delay of about 10 min before the hydrogen concentration maximizes and decays to steady state. In the simultaneous presence of MO (○) and oxygen, the delay in hydrogen production is significantly longer than with MO alone (compare Fig. 5), and the attainable steady state hydrogen concentration lower.

In order to further understand the importance of oxygen in MO decomposition, the photocatalytic decomposition of MO in the absence or presence of MeOH was again followed by UV–vis spectroscopy (Fig. 8a) and LC–MS (Fig. 8b) analysis. Fig. 8a shows that the presence of oxygen significantly prolongs the illumination time needed to achieve full dis-colorization (90 min, compare Fig. 6), while again the presence of MeOH accelerates this, reducing the time needed for full color elimination to 30 min. LC–MS analysis revealed that the intermediate with m/z of 172 was not formed in significant quantities in aerobic conditions after 10 or 30 min of reaction, 30 min being the time at which full dis-colorization was obtained.

4. Discussion

4.1. The necessity of Pt for H_2 evolution from MeOH solutions

In the present study, hydrogen production was not observed, when MO was reacted in anaerobic conditions (in the absence of MeOH), see Fig. 3. While the absence of hydrogen formation for TiO_2 P25 is in agreement with literature [26], several studies have reported formation of hydrogen with simultaneous decomposition of contaminant molecules for Pt containing catalysts [5,15,21]. The absence of hydrogen production with 0.5% Pt–TiO_2 in the present study is probably related to the adsorption and azo-bond cleavage of MO, which likely progresses over Pt sites preferably as compared to proton reduction, inducing reduction of color intensity and the formation of the mass fragment 172 m/z (Fig. 6). We assume that oxidation of water to H_2O_2 is the hole consuming reaction. Contrary to MO, MeOH was efficient in inducing hydrogen formation, small over TiO_2 (maximum at ~0.15 μmol H_2 min^{-1} g^{-1}_{cat}), but significant (~7.5 μmol H_2 g^{-1}_{cat} min^{-1}) over 0.5% Pt–TiO_2 (Fig. 3). The mechanism of MeOH induced hydrogen formation over 0.5% Pt–TiO_2 will be discussed in the following.

4.2. MeOH assisted hydrogen formation

In anaerobic conditions, two reactions of MeOH in aiding the production of hydrogen can be proposed. In the first Reaction (1), MeOH will help to increase the efficiency of proton reduction over Pt by reacting with photogenerated holes, and producing CO [24].

$$CH_3OH(1) + 4h^+ \overset{Pt/TiO_2}{\underset{\lambda=375nm}{\leftrightarrow}} 4H^+ + CO(g) \quad (1)$$

The four protons react over the Pt sites with photo-excited electrons to produce hydrogen. The other light induced reaction is oxidation of MeOH to formaldehyde, occurring over the surface of the TiO_2 nanoparticles, again followed by formation of hydro-

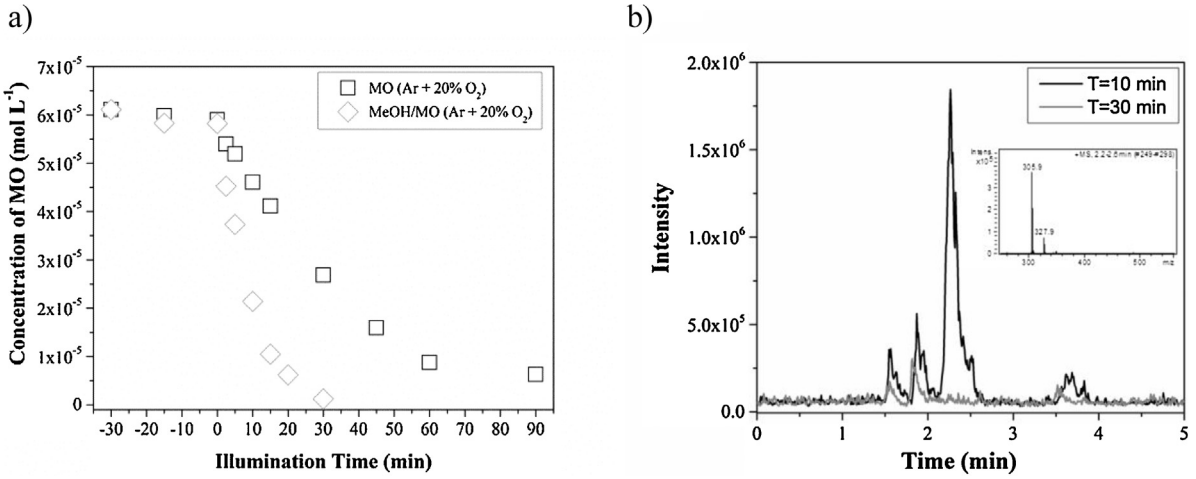

Fig. 8. (a) Photocatalytic decolorization of MO (0.09 mM) in the absence or presence of MeOH (2.48 M) in aerobic conditions (solution saturated with a flow of 5 ml/min of 20% O_2 in Ar for 30 min). (b) Analytical analysis by LC–MS from the sample with MeOH after 30 min illumination.

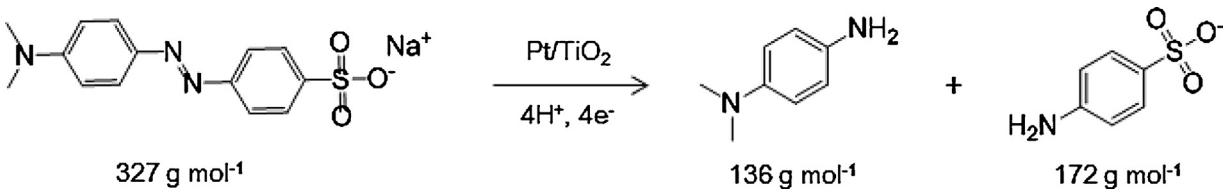

Fig. 9. First step in MO photocatalytic degradation, and possible fragments formed by azo-bond cleavage.

gen by reduction of protons over the Pt sites. The overall process is represented by Reaction (2) [9,15,22].

$$CH_3OH(1) \underset{\lambda=375nm}{\overset{Pt/TiO_2}{\leftrightarrow}} H_2CO(1) + H_2(g) \quad (2)$$

Finally, consecutive reactions of formaldehyde to formic acid (3), and formic acid to CO_2 (4) have also been proposed to contribute to hydrogen formation in anaerobic (reductive) conditions.

$$H_2CO(g) + H_2O(1) \underset{\lambda=375\ nm}{\overset{Pt/TiO_2}{\leftrightarrow}} HCO_2H(1) + H_2(g) \quad (3)$$

$$HCO_2H(1) \underset{\lambda=375nm}{\overset{Pt/TiO_2}{\leftrightarrow}} CO_2(g) + H_2(g) \quad (4)$$

From the catalytic data reported in the present study, we cannot discriminate which of the products of methanol conversion is most important. However, we anticipate Reaction (1) is relevant, based on the initial transient in hydrogen production rate. We speculate this initially decreasing rate is related to poisoning of Pt sites by CO formed in the (partial) oxidation mechanism by Reaction (1). CO is a well-known poison for Pt anodes in direct methanol fuel cells (DMFC) and in fact is reported to prevent the commercial application thereof [27,28]. At some point the extent of poisoning, and competing hydrogenation reactions are apparently in equilibrium, and the hydrogen formation rate reaches steady state.

4.3. Explaining H_2 formation transients from MeOH and MO mixtures in anaerobic conditions

Some remarkable observations regarding the MeOH induced hydrogen formation in the presence of MO at anaerobic conditions can be made (Fig. 5): (i) hydrogen formation is delayed by the presence of MO at concentrations larger than 0.06 mM, (ii) the maximum in hydrogen formation is enhanced in quantity and shows a slower transient to steady state, and (iii) MO dis-colorization is faster in the presence, than in the absence of MeOH. These observations confirm that the Pt catalyst is substrate selective with favorable affinity for MO as compared to protons, as previously indicated in Section 4.1. The reductive discolorization reaction is illustrated in Fig. 9.

Since no other intermediates were observed which could be assigned to possible MeOH–MO reactions, we assume the explanation for acceleration of N=N hydrogenation induced by MeOH is similar to the explanation for hydrogen formation, and due to favorable hole scavenging and occurrence of Reaction (1). Once MO has fragmented, the Pt surface is available for proton reduction to produce hydrogen, explaining the concurrent rise in hydrogen production with the decreasing color intensity of MO. What is obvious is that MO fragments (Fig. 9) enhance the maximum attainable hydrogen production in the presence of MeOH. We speculate this might be related to sulfate formation on the TiO_2 surface by consecutive oxidation of e.g. mass fragment m/z 172. Sulfate formation has been previously reported to promote activity and photonic efficiency. Sulfates can efficiently react with holes generating sulfate radicals, thus improving the apparent quantum efficiency by avoid-

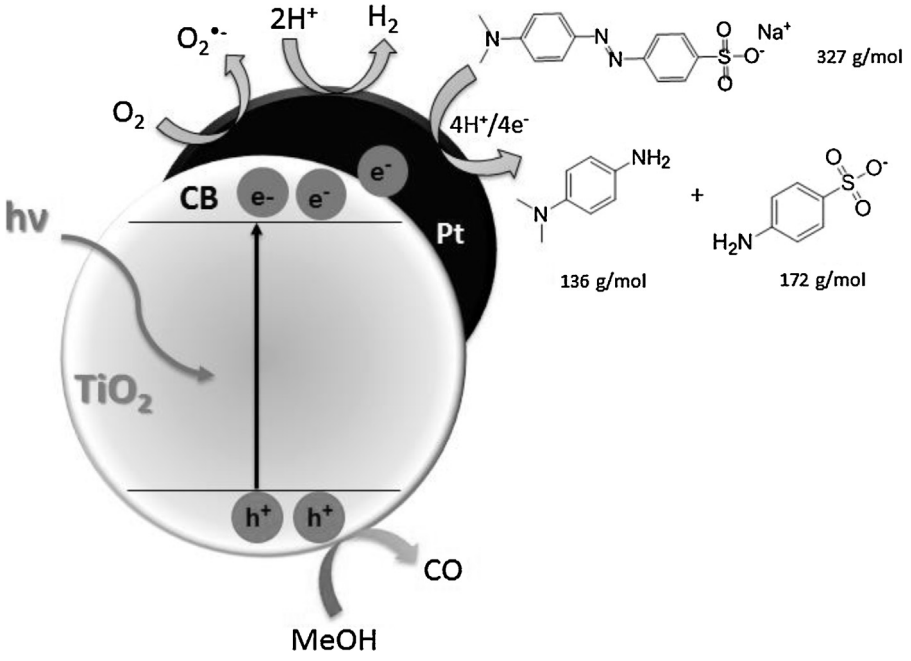

Fig. 10. Schematic representation of all the reduction reactions that occur on the Pt surface, and the (simplified) oxidative MeOH conversion.

ing electron–hole recombination, and likely enhancing methanol oxidation rates [29–31].

4.4. Explaining H_2 formation transients from MeOH and MO mixtures in oxygen lean conditions

Dissolved oxygen delays MO dis-colorization, as well as hydrogen evolution observed in Figs. 7 and 8. The significant delay by the presence of oxygen in the dis-colorization of MO is in agreement with the hypothesis that dis-colorization needs photogenerated electrons and occurs reductively over Pt sites (Fig. 10). We anticipate that oxygen competes for these electrons. The fate of the superoxide and hydroperoxyl radicals formed by reduction of oxygen [13], is likely to react with MeOH, rather than MO, given the significantly higher concentration of MeOH. After the delay, oxygen in solution is mostly converted and the reactions follow the processes discussed for anaerobic conditions. We assume that the acceleration of MO dis-colorization induced by MeOH is again due to favorable hole scavenging, enhancing apparent quantum efficiency. This lowers the concentration of MeOH, on which hydrogen formation was demonstrated to be dependent in Fig. 4, and thus explains the lower steady state hydrogen production rates.

5. Conclusions

The data reported in this study demonstrate that photon–electron stimulated Pt nanoparticles have multiple catalytic functions. The following order in reactant selective reduction activity was observed experimentally: O_2 > MO > H^+. This order in reactivity is based on: (i) MeOH induced hydrogen formation is inhibited by the presence of MO, and (ii) MO dis-colorization and hydrogen formation (by H^+ reduction) are negatively affected by the presence of oxygen. We demonstrate that MeOH is oxidatively converted by reaction with holes, diminishing probability of electron–hole pair recombination, and explaining the promotion in the dye dis-colorization reaction (both in the absence or presence of oxygen). CO is likely a dominant product of MeOH oxidation in anaerobic conditions, in agreement with CO poisoning of Pt being at the origin of the frequently observed maximum in hydrogen production. For practical application of concomitant methanol induced hydrogen formation and dye degradation, Pt/TiO_2 induced photocatalysis is not practically feasible, due to the strong reactant selective activity of the Pt nanoparticles. Moderation of the Pt particles, e.g. by alloying, allowing simultaneous, rather than consecutive processing of oxygen reduction, dye conversion, and production of hydrogen, might lead to improvements. At the same time, the photonic efficiency of dye degradation might be improved by combining TiO_2 with favorable semiconductor substrates, such as silicon, commonly used in construction of photocatalytic microreactors.

Acknowledgements

This work is supported by NanoNextNL, a micro and nanotechnology consortium of the Government of the Netherlands and 130 partners.

References

[1] M.J.M. Bueno, M.J. Gomez, S. Herrera, M.D. Hernando, A. Aguera, A.R. Fernandez-Alba, Environ. Pollut. 164 (2012) 267–273.
[2] M.D.o. Health, Minnesota Drinking Water 2015, Annual Report for 2014, Environmental Health Division, http://www.health.state.mn.us/divs/eh/water/, 2015, pp. 7–11.
[3] J.S. Romão, M.S. Hamdy, G. Mul, J. Baltrusaitis, J. Hazard. Mat. 282 (2015) 208–215.
[4] M.N. Chong, B. Jin, C.W.K. Chow, C. Saint, Water Res. 44 (2010) 2997–3027.
[5] D.I. Kondarides, V.M. Daskalaki, A. Patsoura, X.E. Verykios, Catal. Lett. 122 (2008) 26–32.
[6] Y.X. Li, G.X. Lu, S.B. Li, Chemosphere 52 (2003) 843–850.
[7] Y. Zhao, J.A. Baeza, N. Koteswara Rao, L. Calvo, M.A. Gilarranz, Y.D. Li, L. Lefferts, J. Catal. 318 (2014) 162–169.
[8] S.K. Lee, A. Mills, Platin. Met. Rev. 47 (2003) 61–72.
[9] L.M. Ahmed, I. Ivanova, F.H. Hussein, D.W. Bahnemann, Int. J. Photoenergy (2014).
[10] X.L. D.Y.C. Leung, C.F. Fu, M. Wang, M.K.H. Ni, X.X. Leung, X.Z. Fu Wang, ChemSusChem 3 (2010) 681–694.
[11] P. Pichat, New J. Chem. 11 (1987) 135–140.
[12] O.K. Dalrymple, D.H. Yeh, M.A. Trotz, J. Chem. Technol. Biot. 82 (2007) 121–134.
[13] V.W. Atul, G.S. Gaikwad, M.G. Dhonde, N.T. Khaty, S.R. Thakare, Res. J. Chem. Environ. 17 (2013) 84–94.
[14] R. Baba, S. Nakabayashi, A. Fujishima, K. Honda, J. Phys. Chem. 89 (1985) 1902–1905.
[15] M.K. Jeon, J.W. Park, M. Kang, J. Ind. Eng. Chem. 13 (2007) 84–91.
[16] Y. Li, G. Lu, S. Li, Appl. Catal. A: Gen. 214 (2001) 179–185.
[17] A. Patsoura, D.I. Kondarides, X.E. Verykios, Catal. Today 124 (2007) 94–102.
[18] N.-L. Wu, M.-S. Lee, Int. J. Hydrogen Energ. 29 (2004) 1601–1605.
[19] M.R. St. John, A.J. Furgala, A.F. Sammells, J. Phys. Chem. 87 (1983) 801–805.
[20] K.L. Miller, C.W. Lee, J.L. Falconer, J.W. Medlin, J. Catal. 275 (2010) 294–299.
[21] A. Patsoura, D.I. Kondarides, X.E. Verykios, Appl. Catal. B—Environ. 64 (2006) 171–179.
[22] A. Galinska, J. Walendziewski, Energy Fuels 19 (2005) 1143–1147.
[23] J. Kim, C.W. Lee, W. Choi, Environ. Sci. Technol. 44 (2010) 6849–6854.
[24] A. Mills, S.K. Lee, Platin. Met. Rev. 47 (2003) 2–12.
[25] C.-C. Yang, J. Vernimmen, V. Meynen, P. Cool, G. Mul, J. Catal. 284 (2011) 1–8.
[26] K. Lalitha, J.K. Reddy, M.V. Phanikrishna Sharma, V.D. Kumari, M. Subrahmanyam, Int. J. Hydrogen Energ. 35 (2010) 3991–4001.
[27] C.-C. Ting, C.-H. Liu, C.-Y. Tai, S.-C. Hsu, C.-S. Chao, F.-M. Pan, J. Power Sources 280 (2015) 166–172.
[28] M. Watanabe, S. Motoo, J. Electroanal. Chem. 60 (1975) 267–273.
[29] K. D. Sun, Z. Wang, R. Li Xu, J. Rare Earths 33 (2015) 491–497.
[30] L.G. Devi, M.L. ArunaKumari, J. Mol. Catal. A: Chem. 391 (2014) 99–104.
[31] P.V.R.K. Ramacharyulu, J. Praveen Kumar, G.K. Prasad, B. Sreedhar, Mater. Chem. Phys. 148 (2014) 692–698.